PHYSICAL REVIEW B **107**, 115108 (2023)

Doping as a tuning mechanism for magnetothermoelectric effects to improve zT in polycrystalline NbP

Eleanor F. Scott,[1] Katherine A. Schlaak,[1,2] Poulomi Chakraborty,[3] Chenguang Fu,[4,5] Satya N. Guin,[5,6]
Safa Khodabakhsh,[1] Ashley E. Paz y Puente,[1] Claudia Felser,[5] Brian Skinner,[3] and Sarah J. Watzman[1,*]
[1]*Department of Mechanical and Materials Engineering, University of Cincinnati, Cincinnati, Ohio 45221, USA*
[2]*Department of Physics, University of Cincinnati, Cincinnati, Ohio 45221, USA*
[3]*Department of Physics, The Ohio State University, Columbus, Ohio 43210, USA*
[4]*Department of Materials Science and Engineering, Zhejiang University, Hangzhou 310027, China*
[5]*Max Planck Institute for Chemical Physics of Solids, Dresden 01187, Germany*
[6]*Department of Chemistry, Birla Institute of Technology and Science, Pilani–Hyderabad Campus, Hyderabad 500078, India*

(Received 30 June 2022; revised 22 November 2022; accepted 9 February 2023; published 3 March 2023)

Weyl semimetals combine topological and semimetallic effects, making them candidates for interesting and effective thermoelectric transport properties. Here, we present experimental results on polycrystalline NbP, demonstrating the simultaneous existence of a large Nernst effect and a large magneto-Seebeck effect, which is typically not observed in a single material at the same temperature. We compare transport results from two polycrystalline samples of NbP with previously published work, observing a shift in the temperature at which the maximum Nernst and magneto-Seebeck thermopowers occur, while still maintaining thermopowers of similar magnitude. Theoretical modeling shows how doping strongly alters both the Seebeck and Nernst magnetothermopowers by shifting the temperature-dependent chemical potential, and the corresponding calculations provide a consistent interpretation of our results. Thus, we offer doping as a tuning mechanism for shifting magnetothermoelectric effects to temperatures appropriate for device applications, improving zT at desirable operating temperatures. Furthermore, the simultaneous presence of both a large Nernst and magneto-Seebeck thermopower is uncommon and offers unique device advantages if the thermopowers are used additively. Here, we also propose a unique thermoelectric device that would collectively harness the large Nernst and magneto-Seebeck thermopowers to greatly enhance the output and zT of conventional thermoelectric devices.

DOI: 10.1103/PhysRevB.107.115108

I. INTRODUCTION

Topological materials have attracted much interest in the field of solid-state physics since their discovery, with recent work showing that Dirac semimetals and Weyl semimetals (WSMs) are excellent candidates for both longitudinal and transverse magnetothermoelectric transport applications, including the conversion of waste heat to useful electric power [1–13]. Because WSMs are two-carrier systems, it was predicted that these materials would possess a very large Nernst effect and a minimal Seebeck effect. However, WSMs were also theoretically predicted to possess thermomagnetic transport signatures beyond that found in classical semimetals due to their ultrahigh-mobility charge carriers found in Dirac bands and their bulk Weyl nodes [14,15].

The Seebeck effect is the conventional, longitudinal thermoelectric (TE) effect, while the Nernst effect is its transverse counterpart. In a longitudinal geometry, charge carriers condense on the cold side of the material, making it such that the contributions of oppositely charged carriers effectively cancel each other. Because of this, conventional TE materials are typically single-carrier systems. In contrast, the Nernst effect is produced by applying a magnetic field perpendicular to the applied temperature gradient, producing a Lorentz force and thus a resultant electric field in the mutually orthogonal direction. This magnetic field causes charge separation in the direction of the resulting electric field, meaning the contributions of oppositely signed charge carriers are effectively combined. Therefore, two-carrier systems are expected to possess a large Nernst effect [16]. Although this transverse geometry requires a magnetic field, the temperature gradient and resulting electric field are ultimately decoupled, which provides geometrical freedom in engineering devices [17]. Furthermore, WSMs are predicted to simultaneously exhibit a large magneto-Seebeck effect due to their gapless band structure not seen in traditional semimetals [18,19]. Because both longitudinal and transverse TE voltage can be produced in the presence of a magnetic field, this class of material presents a unique opportunity to utilize magnetothermoelectric effects.

Recent experimental results [1,2,20] have led this research to focus on the WSM NbP, a type I WSM that breaks inversion symmetry [21]. Previous work in single-crystalline NbP observed an unprecedentedly large Nernst thermopower, exceeding 800 $\mu\mathrm{V\,K^{-1}}$ at 109 K and 9 T [1]. Initial work in polycrystalline NbP found that a large Nernst thermopower was maintained, $\sim 90\,\mu\mathrm{V\,K^{-1}}$ at 136 K and 9 T, and a

---

[*] Author to whom all correspondence should be addressed: watzmasj@ucmail.uc.edu

competitive Nernst power factor was observed over a broad temperature range of approximately 100–200 K [2]. This large Nernst thermopower and Nernst power factor were also generally maintained as Nb vacancies were introduced in off-stoichiometric polycrystalline NbP samples [20]. While these results are motivating, they currently show that TE properties are only maximized at high magnetic fields and cryogenic temperatures with moderate TE figures of merit (zT). Here, we focus on polycrystalline, rather than single-crystalline, NbP since polycrystalline samples are more durable, less expensive, and easier to synthesize, making them better-suited for TE device applications, especially as previous results demonstrate a large Nernst power factor in polycrystalline NbP [2,20]. We demonstrate that NbP has not only a large Nernst effect but also a comparably large magneto-Seebeck effect, an unusual feature to find coexisting in semimetallic materials. With the groundwork of previous studies on NbP in mind, this work focuses on what and how material properties can be altered determining appropriate tuning mechanisms to maximize TE effects, and thus zT, in NbP. We offer this research as evidence for doping, and thus altering the temperature-dependent chemical potential, as a tuning mechanism for increasing magnetothermoelectric transport and the temperature range over which it is maximized in NbP. Additionally, we propose a TE device utilizing a simultaneously large magneto-Seebeck and Nernst effect, which offers the potential of increasing device zT by nearly fourfold.

II. EXPERIMENTAL METHODS

Polycrystalline NbP samples were synthesized via direct reaction using powders of niobium and phosphorus. NbP powder was formed into a solid ingot using spark plasma sintering [2], with an approximate density of 90%. Two separate bar-shaped samples were cut from the sintered ingot to be used in transport measurements. Two bars of NbP were selected for analysis: Sample 1 was left unannealed with an average grain size of 2.18 μm, and Sample 2 was annealed at 1000 °C for 1 week, which resulted in an increased average grain size of 3.08 μm. Sample 2 was wrapped in Nb foil with excess NbP powder then encapsulated in a quartz tube which had been purged with argon and then sealed in a vacuum. The average grain size of both samples was found using electron backscattering diffraction (EBSD) on a scanning electron microscope (SEM). The stoichiometry of both samples was estimated using EDS. This revealed that Sample 2 lost phosphorus during the annealing process leaving it as Nb-rich. This was also confirmed in the calculated charge-carrier concentration of both samples, explained further in the supplemental material [22]. The mean free path of NbP was estimated to be $\approx$ 30 nm, which is much smaller than the average grain size of both samples, therefore the transport differences between Sample 1 and Sample 2 are attributed primarily to the differences in stoichiometry and not grain size.

All transport measurements were completed on a 9 T Quantum Design DynaCool Physical Property Measurement System (PPMS). The thermal conductivity, electrical resistivity, Seebeck effect, and Nernst effect were measured using the thermal transport option (TTO) in the conventional one-heater two-thermometer configuration, with the exception of Sample 2′s 9 T electrical resistivity, which was measured on the electrical transport option (ETO). Electrical resistivity and thermal conductivity were measured using MultiVu, Quantum Design’s proprietary software for the PPMS. Both the Seebeck effect and the Nernst effect were characterized using a home-built electrical breakout system with external electronics and customized controls code written in LabVIEW. The magneto-Seebeck effect was characterized in both steady-state and sweeping magnetic fields, while the Nernst effect was characterized in a sweeping magnetic field. The Hall effect was measured with the PPMS’s ETO using the van der Pauw method. Thermoelectric transport data for both the Seebeck and Nernst effects presented in this work were measured isothermally, as opposed to using a conventional adiabatic sample mount where heat flow is unrestricted in the sample and the temperature gradient is not necessarily parallel to only the direction in which it is applied. Isothermal preparation was necessary due to the large thermal Hall effect in NbP, which causes a parasitic temperature gradient to occur when a magnetic field is applied. Further information on isothermal sample preparation for TE measurements can be found in the supplemental material [22] (see also Refs. [23,24] therein).

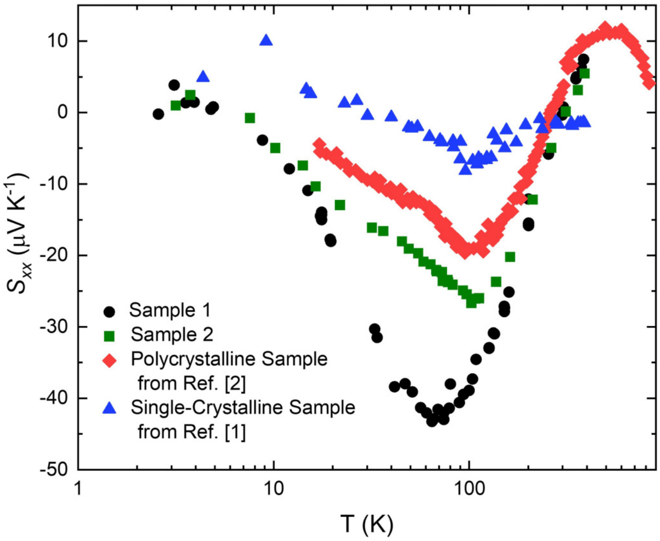

FIG. 1. Comparison of the temperature dependence of the thermopower, S_{xx}, in NbP.

III. EXPERIMENTAL RESULTS

The data presented here follow conventional labeling in order to define the transport geometry using the subscript indices “*abc*,” where a is the direction of the applied flux, b is the direction of the measured field, and c is the direction of the externally applied magnetic field (if present) [17]. Any value with the c index dropped indicates that no magnetic field was applied.

The temperature dependence of the Seebeck effect was measured and reported as a thermopower, S_{xx}, in Fig. 1. All data presented were measured isothermally, except for the polycrystalline sample from Ref. [2], which was measured adiabatically. The Seebeck effect of NbP Sample 1 resulted in a maximum magnitude of thermopower of 43.3 μV K^{-1} at

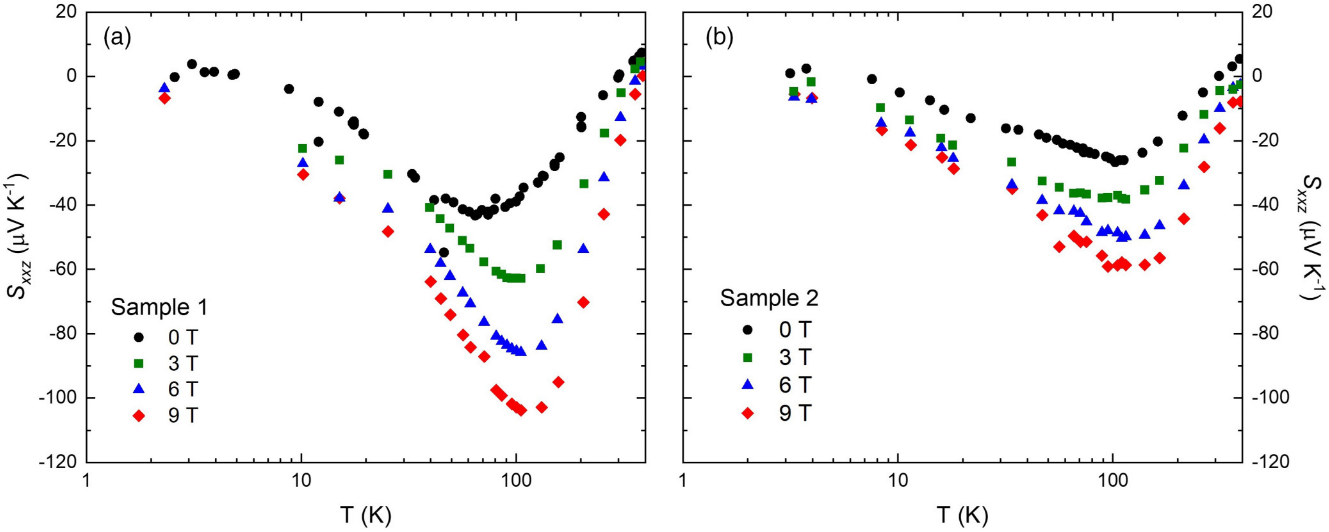

FIG. 2. Temperature dependence of the magneto-Seebeck thermopower, S_{xxz}, at discrete magnetic fields in polycrystalline NbP for (a) Sample 1 and (b) Sample 2.

64.5 K, and Sample 2 resulted in a maximum magnitude of thermopower of 26.7 μV K^{-1} at 102.5 K. In comparison, the polycrystalline sample studied in Ref. [2] reached a maximum magnitude of thermopower of ~ 20 μV K^{-1} near 95 K, and the single-crystalline sample from Ref. [1] had a maximum magnitude of thermopower of only ~ 8 μV K^{-1} near 100 K. All three NbP polycrystalline samples have a thermopower significantly exceeding that of the single-crystalline sample. Furthermore, the temperature at which the maximum magnitude of thermopower occurs changes from sample to sample, with the most significant difference being that between Samples 1 and 2.

A large magneto-Seebeck effect, S_{xxz}, was observed in both Samples 1 and 2 with the magnetic field applied perpendicular to the directions of both the applied heat flux and measured electric field; this is shown as a function of temperature at discrete magnetic fields in Fig. 2. S_{xxz} increased in magnitude as a function of magnetic field up to 9 T, more than doubling the maximum magnitude of thermopower in comparison to the 0 T results. A maximum magnitude of thermopower of 103.8 μV K^{-1} at 105.4 K, 9 T was observed in Sample 1, and a maximum magnitude of thermopower of 59.1 μV K^{-1} at 94.77 K, 9 T was observed in Sample 2. Once again, the maximum values of S_{xxz} differ between the samples, and the temperature at which the maximum occurs increases with an increase in externally applied magnetic field for Sample 1. Most notable, though, is the presence of the large isothermal magneto-Seebeck effect in the polycrystalline NbP samples studied in this work. In comparison, previous work in single-crystalline NbP observed no measurable isothermal magneto-Seebeck effect [1], although an adiabatic magneto-Seebeck effect was observed and attributed to parasitic contributions from the Nernst effect into the magneto-Seebeck effect as seen in the supplemental material of Ref. [1]; only adiabatic results for the magneto-Seebeck effect have been previously reported in polycrystalline NbP [2].

The Nernst thermopower, S_{xyz}, in both Samples 1 and 2, shown as a function of magnetic field at select temperature in Fig. 3, was found to be on the same order of magnitude as the magneto-Seebeck thermopower. S_{xyz} in Samples 1 and 2 is comparable to that of polycrystalline NbP in Ref. [2], demonstrating that, although S_{xyz} is large in polycrystalline NbP, it is reduced by at least an order of magnitude from the huge Nernst thermopower observed in single-crystalline NbP [1]. Sample 1 has a maximum Nernst thermopower of 51.6 μV K^{-1} at 159.1 K, 9 T, while Sample 2 has a maximum Nernst thermopower of 99.7 μV K^{-1}, at 163.8 K, 9 T. Both the magnitudes of the Nernst thermopower and the temperature at which they occur differ between the two samples. The Nernst thermopower as a function of magnetic field also exhibits two distinct slopes, a high-field region between $|3\ \mathrm{T}|$ and $|9\ \mathrm{T}|$ and a low-field region below $|2\ \mathrm{T}|$, behavior that is consistent with previously work in NbP [1,2].

The temperature dependence of the electrical resistivity for Samples 1 and 2 is shown in Fig. 4. In the polycrystalline samples, the electrical resistivity is increased from that of the single crystal [1], although the electrical resistivity is still comparable in order of magnitude to that of a conventional metal. The temperature dependence of thermal conductivity is shown in Fig. 5, indicating a strong reduction in thermal conductivity of polycrystalline NbP as compared to single-crystalline NbP. This, combined with the relatively low electrical resistivity, ultimately lends itself to being advantageous for using polycrystalline NbP in thermoelectric applications to increase the thermoelectric figure of merit, zT.

IV. THEORETICAL RESULTS AND DISCUSSION

A combined look at the key transport values for Samples 1 and 2, compared to previously published data for NbP, is shown in Table I.

Reference [1] determined that as the chemical potential moved with temperature, it eventually approached the energy of the Weyl points, where it became pinned due to a minimum density of states in the Dirac bands. In a type I WSM, the energy of the Weyl points is also the location where NbP is

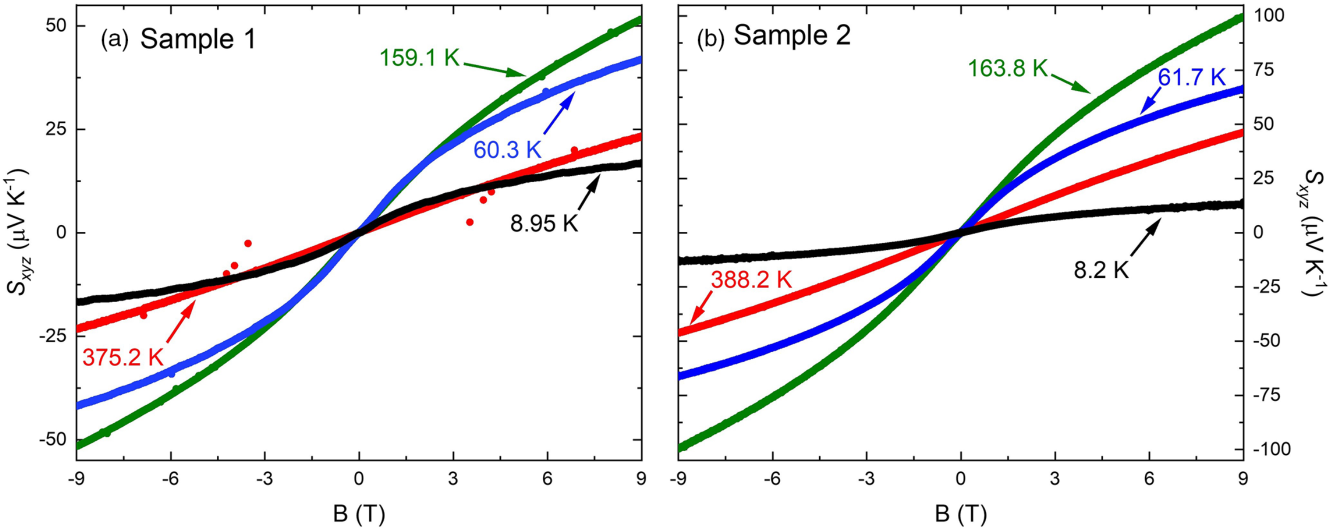

FIG. 3. Magnetic-field dependence of the Nernst thermopower, S_{xyz}, at discrete temperatures in polycrystalline NbP for (a) Sample 1 and (b) Sample 2.

fully compensated. In single-crystalline NbP, both the thermopowers S_{xx} and S_{xyz} were maximized (in magnitude) at a temperature $T \approx 100$ K, which is close to the temperature at which the chemical potential begins to shift strongly toward the energy of the Weyl points. In the polycrystalline Samples 1 and 2, the maximum magnitude of S_{xx} for Sample 1 occurs at 64.50 K and the maximum magnitude for Sample 2 occurs at 102.5 K, differing from the single crystal. The maximum S_{xyz} from the Nernst effect, though, occurs at larger temperatures, with the maximum S_{xyz} of Sample 1 occurring at 159.1 K and the maximum of Sample 2 occurring at 163.8 K. The temperatures at which these maxima occur differ between samples, indicating that the samples encompass differing temperature dependences of their chemical potentials and thus their Fermi levels. Additionally, the charge-carrier concentrations differ by more than a factor of 10^{17} cm^{-3} and the charge-carrier mobilities differ by an order of magnitude in the 0 K limit (see Table SI of the supplemental material [22]). Because the Fermi level can be manipulated via doping, this difference offers evidence that both the maximum magnitude of thermopower and the temperature at which it occurs can be tuned via doping.

To provide a theoretical interpretation of our results, we perform calculations of both S_{xxz} and S_{xyz} arising from a Weyl electron band. These calculations assume an ideal, gapless, linear Weyl dispersion with constant Fermi velocity v_F. Our calculations use the Boltzmann transport description, which is valid in the semiclassical limit where the electron system is far from the extreme quantum limit of magnetic field. Since previous work [1] has determined that Weyl bands dominate transport in NbP, only contributions from the Weyl bands are considered in our theoretical results; however, topologically trivial bands are known to exist in close proximity to the Weyl bands and could reasonably contribute to transport. We

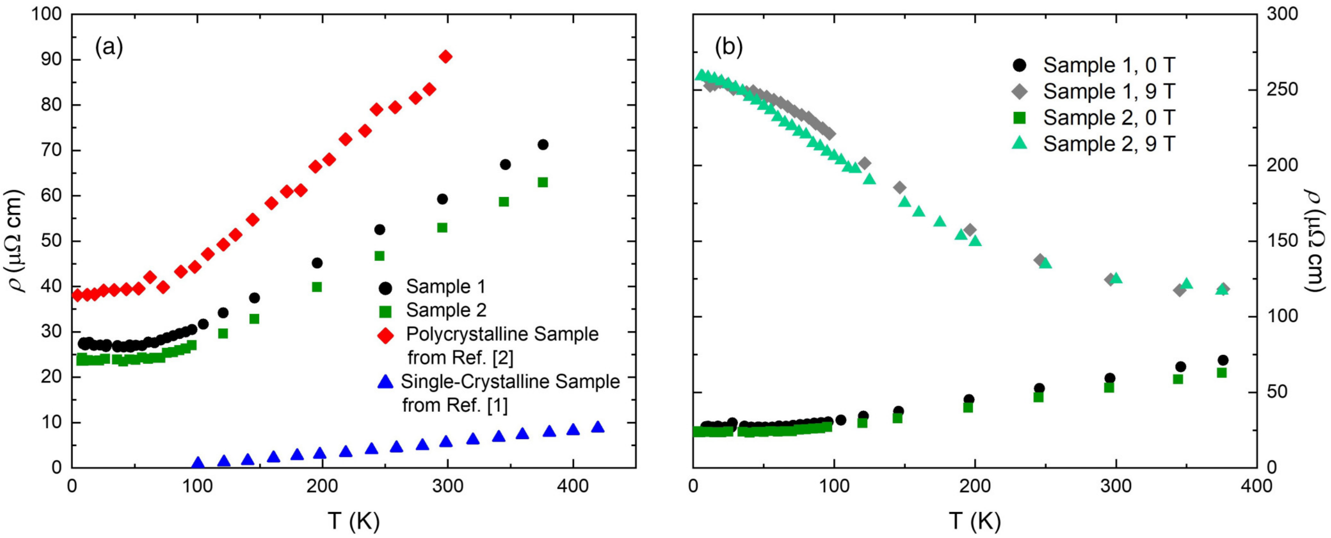

FIG. 4. (a) Temperature dependence of electrical resistivity at 0 T for Samples 1 and 2 compared to previously published data. (b) Temperature dependence of electrical resistivity for Samples 1 and 2 at 0 and 9 T.

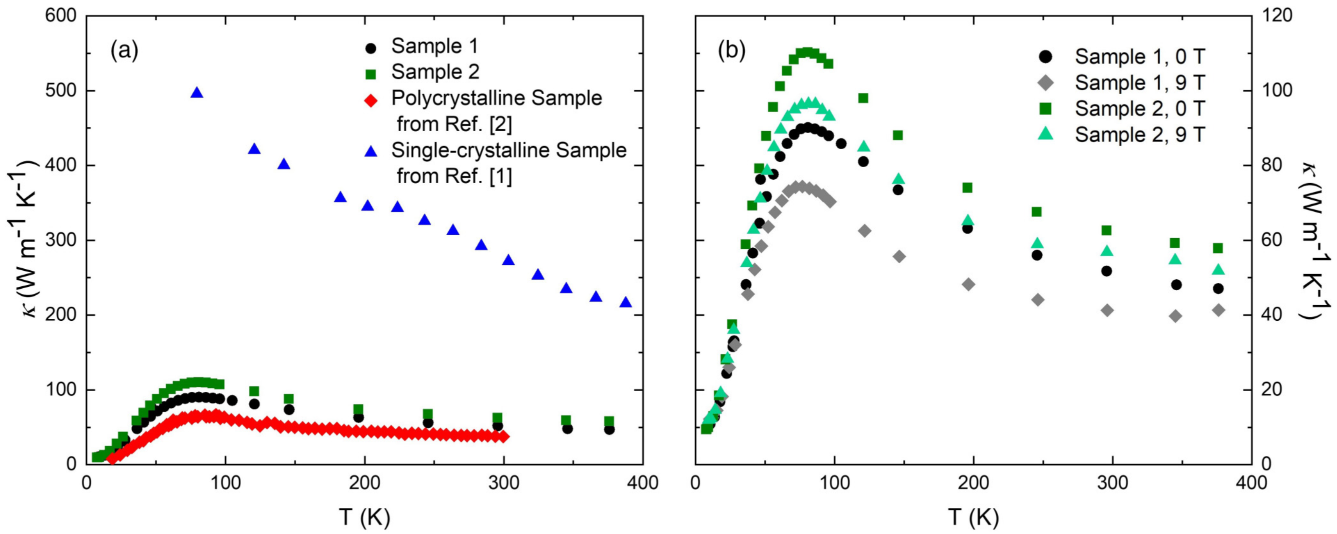

FIG. 5. (a) Temperature dependence of thermal conductivity at 0 T for Samples 1 and 2 compared to previously published data. (b) Temperature dependence of thermal conductivity for Samples 1 and 2 at 0 and 9 T.

discuss some apparent consequences of these trivial bands, which are outside of our theoretical modeling, below. A detailed description of these calculations is provided in the supplemental material [22]. The calculations take as an input the value of the (zero-temperature) Fermi energy E_F (which in general is modified by doping), the transport scattering time τ, and the Fermi velocity v_F. Except where otherwise noted, the theory curves presented in this section use the values of E_F and τ that were estimated for the single-crystalline samples in Ref. [1] [$E_F \approx 8$ meV $= k_B \times$ (92.8 K) and $\tau = 0.3$ ps, respectively], and we have not attempted to fit these parameters to the data. For simplicity, we use a description where τ is an energy-independent constant, and we take v_F to be isotropic and equal to 10^5 m s^{-1}. In the supplemental material [22], we comment on the effect of energy dependence of the scattering rate; in general, the scattering rate alters certain numeric prefactors but does not change any results qualitatively.

At zero magnetic field, and within our approximation of a constant scattering time, the thermopower is given by Eq. (1):

$$S_{xx} = -\frac{k_B}{e}\,\frac{2\pi^2 k_B T \mu}{3\mu^2 + \pi^2 (k_B T)^2}, \qquad (1)$$

where $\mu = \mu(T)$ is the temperature-dependent chemical potential [a full expression for $\mu(T)$ for an isolated Weyl band is given in the supplemental material [22]], with 0 eV defined as the energy of the Weyl points, k_B is the Boltzmann constant, and e is the elementary charge. At low temperatures, the chemical potential approaches a constant value equal to the Fermi energy $E_F = \hbar v_F (6\pi^2 n/g)^{1/3}$, where $\hbar$ is the reduced Planck constant, n is the charge-carrier density at $T = 0$, and g is the degeneracy. Consequently, at low temperatures the magnitude of the thermopower increases linearly with temperature, $S_{xx} \simeq -(k_B/e)(2\pi^2/3)(T/T_F)$, where $T_F \equiv {}^{E_F}/_{k_B}$ is the Fermi temperature. Such growth can be understood, as in usual metals, as a consequence of the linear growth in entropy of the electron system as the temperature is increased due to thermal excitations of electrons around the Fermi surface. On the other hand, at high temperatures $T \gg T_F$, the chemical potential for an isolated Weyl band falls toward zero as $\mu \propto 1/T^2$, and consequently the magnitude of the thermopower decreases as $1/T^3$. This decline at large temperatures is a result of thermally excited holes appearing in the valence band, which cancel the thermopower contribution from electrons. Equation (1) predicts a universal dependence of the thermopower on the ratio T/T_F, with S_{xx} having a maximum magnitude of ≈ 156 μV K^{-1} at a temperature $T \approx 0.35 T_F$. Thus, the prediction of this calculation is that by changing the doping (and therefore the value of T_F), one can set the temperature corresponding to the thermopower maximum, while the value of the maximum peak thermopower is unaffected.

TABLE I. Comparison of maximum values of key TE transport phenomena and corresponding temperatures at which they occur.

NbP sample	Maximum magnitude of S_{xx} at 0 T		Maximum magnitude of S_{xxz} at 9 T		Maximum S_{xyz} at 9 T	
	S_{xx} (μV K^{-1})	T (K)	S_{xxz} (μV K^{-1})	T (K)	S_{xyz} (μV K^{-1})	T (K)
Sample 1	43.3	64.50	103.8	105.4	51.6	159.1
Sample 2	26.7	102.5	59.1	94.77	99.7	163.8
Polycrystalline NbP from Ref. [2]	20	95	50	110	92	136
Single-crystalline NbP from Ref. [1]	8	100	–	–	800	109

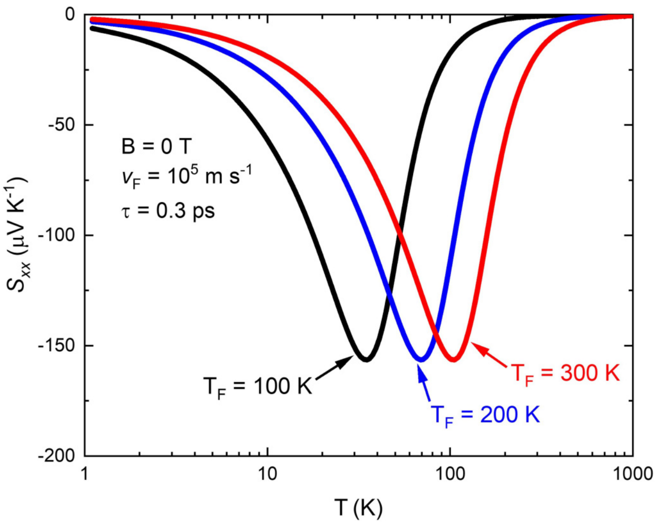

FIG. 6. Theoretical model of S_{xx} at various T_F and 0 T, where $v_F = 10^5$ m s^{-1} and $\tau = 0.3$ ps.

This dependence is shown in Fig. 6. The experimental data in Fig. 1 show a somewhat smaller value of the maximum thermopower, which varies from one sample to the next. This discrepancy may arise from the presence of nearby trivial bands, as we discuss below.

The experimental data in Fig. 1 are consistent with the theoretical result of Eq. (1) at low temperature. Increased doping reduces the slope of S_{xx} versus T. At temperatures higher than ≈ 100 K, however, S_{xx} declines in magnitude rapidly toward zero even for samples with large T_F, and the magnitude of S_{xx} never reaches values as high as the maximum magnitude of ≈ 156 μV K^{-1} as predicted above. At room temperature or higher, the sign of the thermopower is inverted. One possible origin for this discrepancy with the theory relates to the presence of topologically trivial bands, in addition to the Weyl bands dominating transport, in the band structure, which have been predicted based on first-principles calculations [25]. For example, if a trivial n-type band is nearby in energy to the Weyl points, then at elevated temperatures this trivial band has an increased concentration of thermally populated electrons, such that the chemical potential is forced to move below the Weyl point in order to maintain charge neutrality. In this scenario, when the chemical potential crosses through the energy of the Weyl points, the thermopower arising from the Weyl bands rapidly falls to zero, and at higher temperatures the sign of the thermopower is inverted (along with the sign of the Hall coefficient, as we discuss in the supplemental material [22]).

An applied magnetic field tends to enhance the thermopower via the magneto-Seebeck effect. A theoretical calculation for an isolated Weyl band in the limit $T \ll T_F$ gives Eq. (2):

$$S_{xxz} \simeq -\frac{k_B}{e}\frac{\pi^2}{3}\frac{2+3(B/B_0)^2}{1+(B/B_0)^2}\frac{T}{T_F}, \tag{2}$$

where $B_0 = E_F/ev_F^2\tau$. (For reference, at $T_F \sim 100$ K, $v_F \sim 10^5$ m s^{-1}, and $\tau \sim 1$ ps, the magnetic-field scale $B_0 \sim 10$ T.) At sufficiently large magnetic fields $B \gg B_0$, the slope of S_{xxz} versus temperature is increased by a factor of 3/2. At temperatures comparable to T_F, the enhancement by magnetic field is more dramatic. This enhanced magnetothermopower is illustrated in Fig. 7.

When the temperature becomes comparable to T_F, the chemical potential drops toward the energy of the Weyl point, and S_{xxz} falls again as in the zero-field case of S_{xx}. In principle, the growth of S_{xxz} with temperature can continue toward larger temperatures $T \gtrsim T_F$ in cases in which the magnetic field is strong enough to produce a large Hall angle ($\rho_{xyz} > \rho_{xxz}$) [18,19,26]. In this regime, the peak magnetothermopower is parametrically enhanced by the magnetic field, but this large magnetic-field regime is not realized in our experiments.

Finally, we can use our theory to calculate the dependence of the Nernst thermopower, S_{xyz}, on temperature and doping. In general, the magnitude, and even the sign, of the Nernst thermopower depends sensitively on the scattering mechanism and its dependence on the quasiparticle energy. Since we are using a simple model with energy-independent scattering, our theory should be taken only as a general indication of the dependence on temperature and doping. Within this model, S_{xyz} to lowest order in magnetic field can be calculated as

$$S_{xyz} \simeq \frac{k_B}{e}\frac{\pi^2}{3}\frac{B}{B_0}\frac{E_F^2\left(\frac{\pi^2}{3}\mathrm{k}_\mathrm{B}^2\mathrm{T}^2-\mu^2\right)}{\left(\frac{\pi^2}{3}\mathrm{k}_\mathrm{B}^2\mathrm{T}^2+\mu^2\right)^2}\frac{T}{T_F}. \tag{3}$$

(Notice that S_{xyz} remains finite in the limit of zero chemical potential and finite temperature, where both E_F and μ go to zero, since the values of B_0 and T_F are proportional to E_F.) As the temperature is increased, the value of S_{xyz} first increases due to the increased entropy of the charge carriers. At temperatures larger than $\sim T_F$, however, S_{xyz} falls again as $1/T$. Ignoring the presence of any possible trivial bands and inserting the corresponding behavior of $\mu(T)$ gives S_{xyz}, which at low field has a maximum at $T \approx 0.6T_F$. At large magnetic fields $B \gg B_0$, S_{xyz} falls as $1/B$. This behavior of S_{xyz} is shown in Fig. 8.

V. FUTURE OUTLOOK

The simultaneous presence of both a large Nernst effect and a magneto-Seebeck effect, where the thermopowers from each effect are on the same order of magnitude, is not typically found in a single material. In a two-carrier system, the two signs of charge carrier typically counteract each other in a longitudinal geometry as both polarities of charge carriers condense on the cold side. However, the unique band structure of WSMs leads to a large longitudinal TE effect in the presence of a transverse magnetic field [18]. This result implies that, in the presence of a magnetic field, the total effective thermopower of NbP can include contributions from both longitudinal and transverse TE effects, which effectively doubles the total thermopower if a TE device is set up appropriately. Thermoelectric devices using WSMS typically utilize the transverse geometry exclusively due to their large Nernst effect. Yet in WSMs, a large magneto-Seebeck effect also exists concurrently but is unused in transverse devices. Because both transverse and longitudinal effects are simultaneously present in NbP, a thermoelectric device utilizing both could be not only more efficient but also reasonably simplistic. A single leg schematic of such a proposed device is shown in

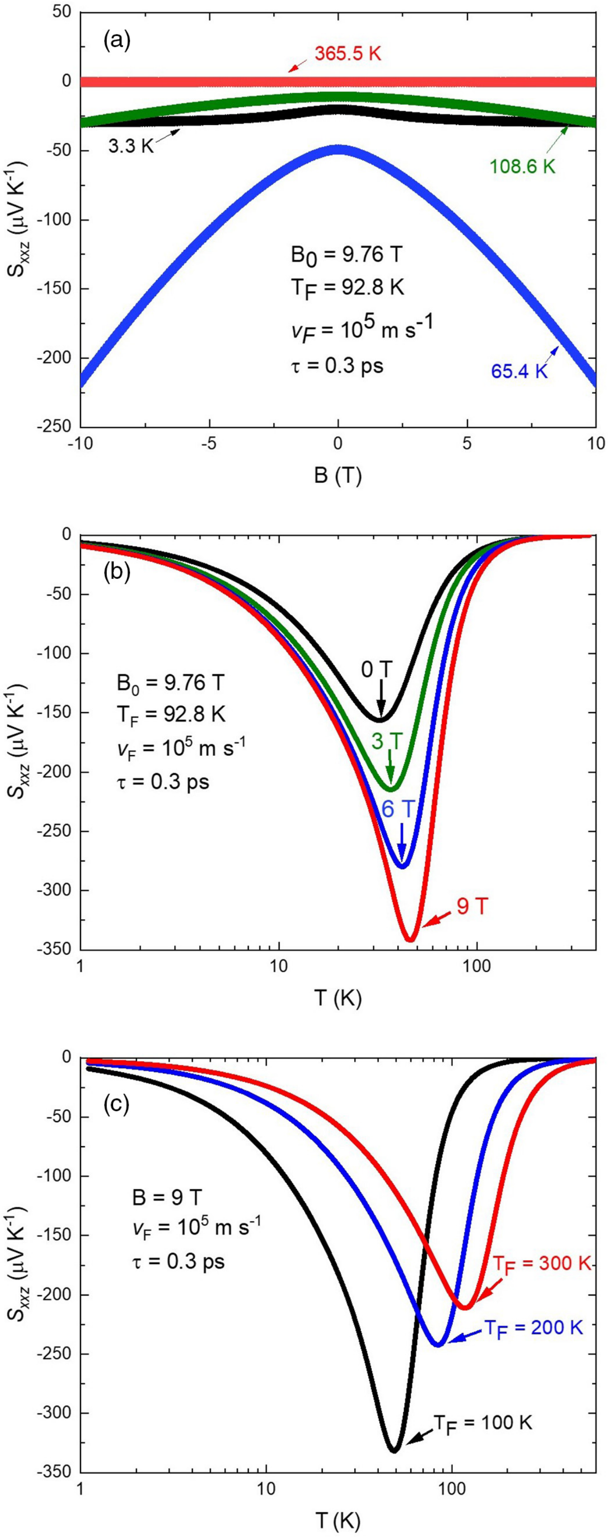

FIG. 7. Theoretical calculations of (a) S_{xxz} as a function of magnetic field at various temperatures, with constant $T_F = 92.8$ K and $B_0 = 9.76$ T; (b) S_{xxz} as a function of temperature at discrete magnetic fields, with constant $T_F = 92.8$ K and $B_0 = 9.76$ T; and (c) S_{xxz} at various T_F and constant $B = 9$ T. For all plots, $v_{\mathrm{F}} = 10^5\ \mathrm{m\,s^{-1}}$ and $\tau = 0.3$ ps.

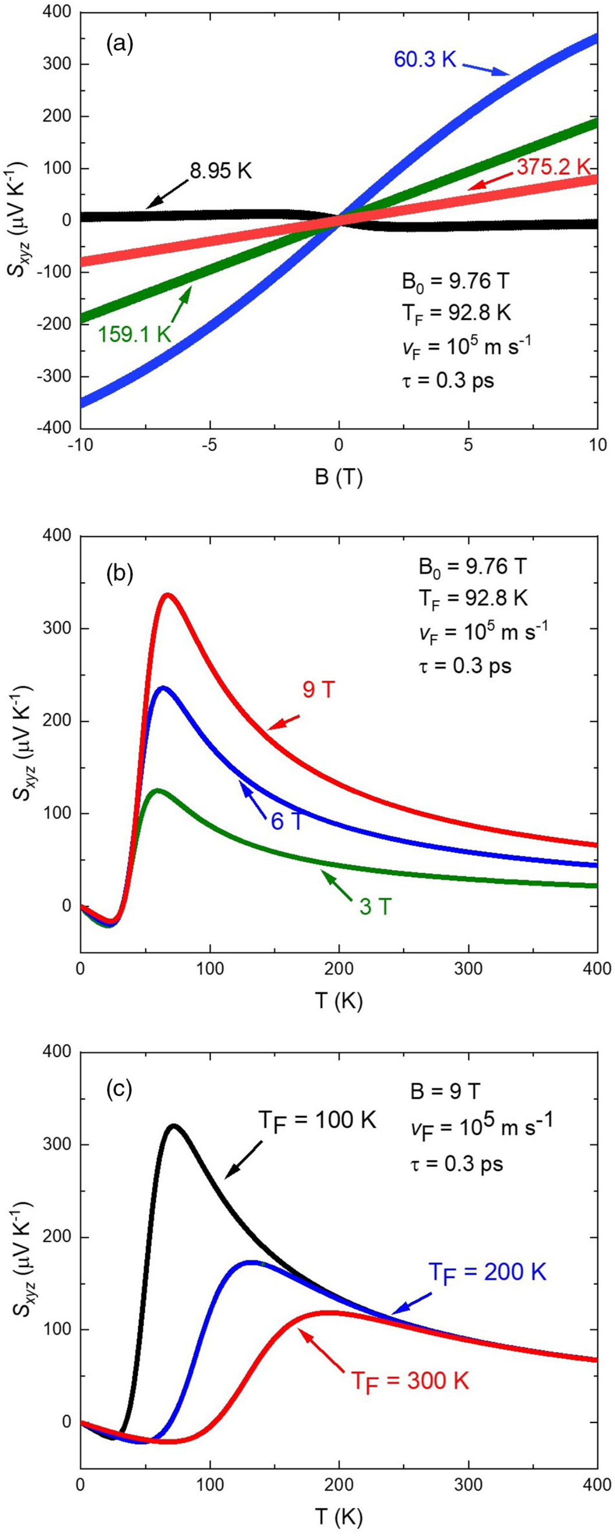

FIG. 8. Theoretical calculations of (a) S_{xyz} as a function of magnetic field at various temperatures, with constant $T_F = 92.8$ K and $\mathrm{B}_0 = 9.76$ T; (b) S_{xyz} as a function of temperature at discrete magnetic fields, with constant $T_F = 92.8$ K and $\mathrm{B}_0 = 9.76$ T; and (c) S_{xyz} at various T_F and constant $B = 9$ T. For all plots, $v_{\mathrm{F}} = 10^5\ \mathrm{m\,s^{-1}}$ and $\tau = 0.3$ ps.

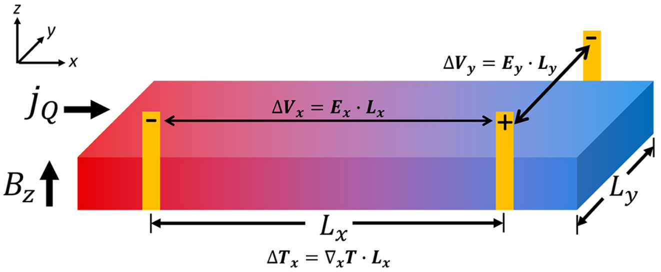

FIG. 9. Schematic of a single TE leg for the proposed device utilizing contributions from both the Nernst and Seebeck effects.

Fig. 9, demonstrating how both the longitudinal and transverse voltage output could be harnessed simultaneously. However, geometrical design optimization would still be necessary for a heterojunction device, where both n-type and p-type TE legs are necessary to return the longitudinal electric field to an isothermal plane for a total longitudinal output voltage. The device would need to be wired in such a way that the voltage outputs of both magneto-Seebeck and Nernst voltages are additive, with only one magnetic field direction being needed for the entire device. We offer Fig. 9 as a concept only, as such a device would need further optimization to operate appropriately.

By calculating the thermoelectric figure of merit, zT, and power factor, PF, the performance enhancement of such a device can be quantified. Calculating zT differs depending on the geometry of the TE transport property used. Because both the magneto-Seebeck and Nernst effects are being utilized, two different zTs and PFs can be calculated. Equations (4) and (5) are the formulas used for calculating longitudinal zT and PF, respectively, from the longitudinal thermopower S_{xxz}:

$$zT_{xxz} = \frac{S_{xxz}^2 \sigma_{xxz}}{\kappa_{xxz}} T, \tag{4}$$

$$PF_{xxz} = S_{xxz}^2 \sigma_{xxz}, \tag{5}$$

Similarly, the method for calculating transverse zT and PF is shown in Eqs. (6) and (7), respectively, using the transverse thermopower S_{xyz}:

$$zT_{xyz} = \frac{S_{xyz}^2 \sigma_{yyz}}{\kappa_{xxz}} T, \tag{6}$$

$$PF_{xyz} = S_{xyz}^2 \sigma_{yyz}. \tag{7}$$

It should be noted that electrical resistivity ρ, which was directly measured, is not mathematically the direct inverse of electrical conductivity σ but a tensor making $\sigma_{xxz} = \frac{\rho_{xxz}}{\rho_{xxz}^2 + \rho_{xyz}^2}$. However, because the Hall resistivity ρ_{xyz} is significantly smaller than the longitudinal electrical resistivity ρ_{xxz} [22], $\sigma_{xxz} \approx \frac{1}{\rho_{xxz}}$. Also, because the samples are polycrystalline, it can reasonably be assumed that the electrical resistivity is isotropic such that $\rho_{xxz} \approx \rho_{yyz}$.

We now define the effective zT and PF produced by the combined use of Nernst and magneto-Seebeck effects using Eqs. (8) and (9), respectively:

$$zT_{\text{effective}} = \frac{(|S_{xyz}| + |S_{xxz}|)^2 \sigma_{xxz}}{\kappa_{xxz}} T, \tag{8}$$

$$PF_{\text{effective}} = (|S_{xyz}| + |S_{xxz}|)^2 \sigma_{xxz}. \tag{9}$$

Here, we add the magnitude of the thermopowers assuming that such a device would be wired in such a way that the voltages are all the same sign when combined. Equations (8) and (9) refer to $zT_{\text{effective}}$ and $PF_{\text{effective}}$ for a single leg of the proposed device, as shown in Fig. 9. However, because a conventional TE device requires two legs (n-type and p-type pair), the actual effective thermopower of the device would be the sum of $|S_{xxz}|$ and $|S_{xyz}|$ from each of the legs. Thus, both a transverse and longitudinal voltage would come from each of the n-type and p-type legs. Furthermore, geometrical device optimization, specifically in the leg cross-sectional area, is not considered here. An advantage of transverse TE devices is that the output scales extrinsically with the device size (i.e., a larger voltage output would result from increasing the device size in the parallel dimension), but longitudinal devices require an optimization in leg cross-sectional area to optimize zT. Since both longitudinal and transverse TE effects are explored in this device, geometrical optimization would be necessary to realistically design such a device.

The resulting zT and PF values of Samples 1 and 2 from Eqs. (4)–(9) are shown in Fig. 10.

zT_{xxz} and PF_{xxz} refer to the longitudinal figure of merit and power factor calculated from the Seebeck effect [Eqs. (4) and (5)], and zT_{xyz} and PF_{xyz} refer to the transverse figure of merit and power factor calculated from the Nernst effect [Eqs. (6) and (7)]. $zT_{\text{effective}}$ and $PF_{\text{effective}}$ were calculated using the isothermal data for S_{xxz} and S_{xyz}, shown in Figs. 2 and 3, respectively, both of which were measured independently and isothermally. The proposed device design in Fig. 9 is inherently adiabatic, therefore the data shown in Fig. 10 should be considered as an estimate only.

When considering all three independent TE effects (Seebeck, magneto-Seebeck, and Nernst effects) observed in this work for Sample 1, zT_{xxz} (9 T) has the largest magnitude of 0.0145 at 196.4 K, which reflects the large magneto-Seebeck effect observed in this material. PF_{xx} (0 T) reached the largest magnitude of 6.7 mW m^{-1} K^{-2} at 47 K. Unfortunately, this power factor drops off to near zero above 200 K. However, PF_{xxz} (9 T) reaches a lower maximum of 5.25 mW m^{-1} K^{-2} at 121 K but does not drop to near zero until $\sim$ 300 K.

Of the TE effects observed in Sample 2, zT_{xyz} (9 T) has the largest magnitude of 0.023 at 250.0 K, which reflects the larger Nernst effect observed in this sample. PF_{xyz} (9 T) reached the largest magnitude of 5.998 mW m^{-1} K^{-2} at 200.0 K. A large PF_{xyz} (9 T) is maintained from $\sim$ 100 to $\sim$ 300 K.

When utilizing both the magneto-Seebeck and Nernst effects simultaneously, the effective thermopower is increased in the proposed device while maintaining the same electrical resistivity and thermal conductivity. This results in $zT_{\text{effective}}$

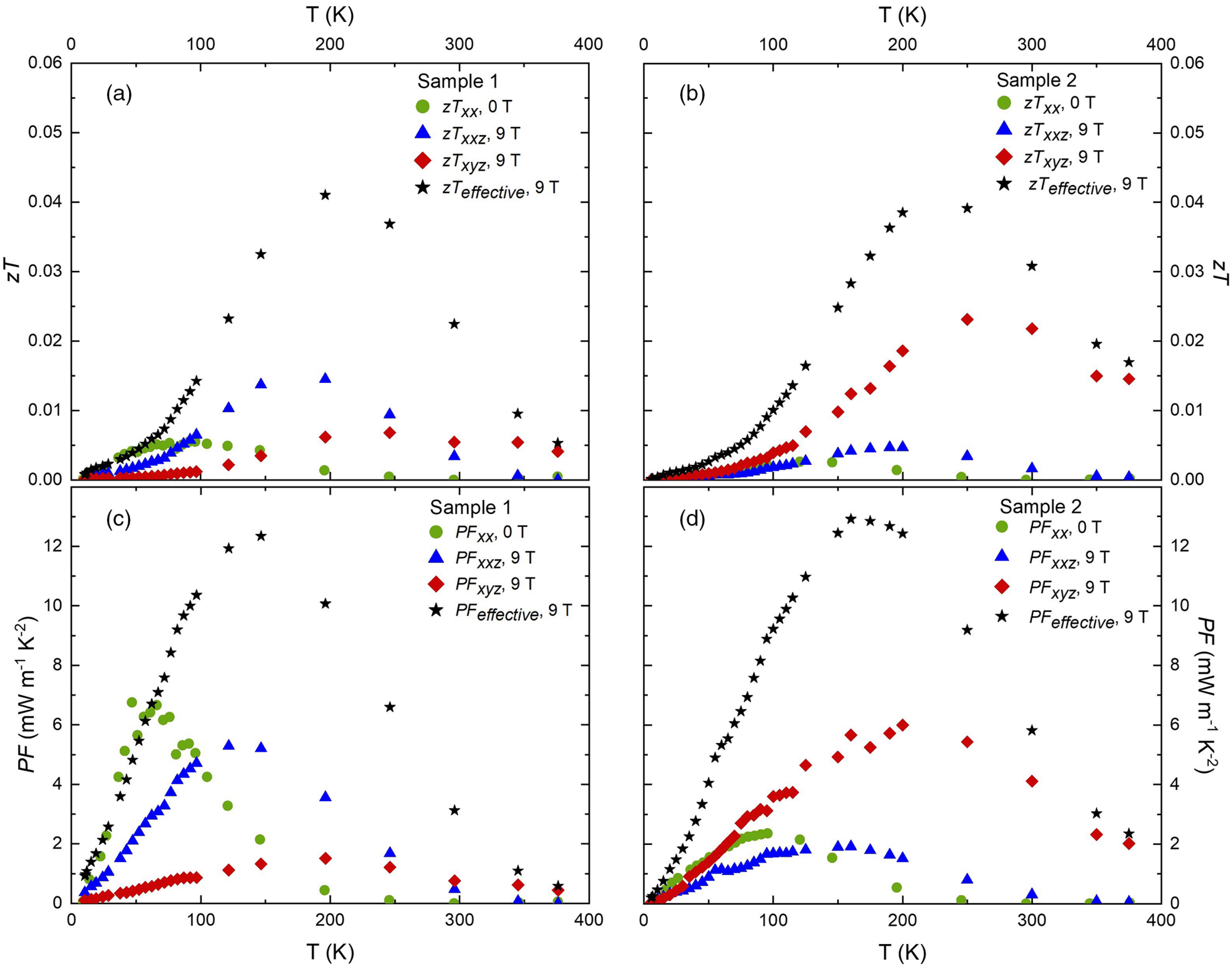

FIG. 10. Temperature dependence of zT and PF in Sample 1 [frames (a) and (b), respectively] and Sample 2 [frames (c) and (d), respectively] with contributions from the Seebeck effect, the magneto-Seebeck effect at 9 T, the Nernst effect at 9 T, and combined longitudinal and transverse effects at 9 T for the proposed device.

(9 T) reaching a maximum of 0.041 at 196.4 K, which is nearly triple in value as compared to the highest figure of merit for an independent TE effect in Sample 1. Similarly, $PF_{\mathrm{effective}}$ (9 T) reaches a maximum of 12.35 mW m^{-1} K^{-2} at 146.5 K, nearly double the maximum power factor for an independent TE effect in Sample 1, and the large power factor is maintained across a large temperature range of approximately 100–200 K.

The $zT_{\mathrm{effective}}$ (9 T) of Sample 2 reaches a maximum of 0.039 at 250.0 K, which is not significantly different from the Sample 1 maximum value, however it occurs at a much higher temperature. Sample 2's $PF_{\mathrm{effective}}$ (9 T) reaches a maximum of 12.91 mW m^{-1} K^{-2} at 160.0 K. Once again, the magnitude does not vary significantly from that of Sample 1, but the temperature at which it occurs has changed. This indicates that tuning the operating temperature of the device by means of tuning T_F via doping will not significantly affect the magnitude of zT or PF of the device.

The $zT_{\mathrm{effective}}$ (9 T) found here for the proposed device is competitive with, and even exceeds, figures of merit found in recent works on TE transport in WSMs. Table II shows the largest zT reported experimentally for other WSMs, where the maximum zT observed by a single TE effect (either Seebeck, magneto-Seebeck, or Nernst effect independently) is zT_{xx} (0 T) = 0.042 at ∼ 80 K in $\mathrm{Mo_{0.92}Nb_{0.08}Te_2}$ [27], which is comparable to the $zT_{\mathrm{effective}}$ of the NbP samples in this work. Similar to the results for polycrystalline NbP reported in this work, $\mathrm{MoTe_2}$ demonstrates significant changes in the maximum zT and temperature at which that maximum occurs —zT_{xx} (0 T) = 0.002 97 at ∼ 20 K for $\mathrm{MoTe_2}$ and zT_{xx} (0 T) = 0.042 at 80 K for $\mathrm{Mo_{0.92}Nb_{0.08}Te_2}$ [27]—offering further evidence that doping can be used as a tuning mechanism to increase zT.

As such, the proposed device offers a pathway to make polycrystalline WSMs competitive for magnetic TE device applications. Worthy of note is that the majority of TE transport literature focuses on single-crystalline samples. Because this work shows a significant difference between the transport properties of polycrystalline NbP compared to single-crystalline NbP, most notably a large isothermal magneto-Seebeck effect present in polycrystalline but not single-crystalline samples, there may be potential for TE

TABLE II. Comparison of zT values from independent TE effects in WSMs. The bold-faced terms represent the largest zT from this work.

Material	Sample type	Max zT	Conditions	Reference
NbP, Sample 1	Polycrystalline	0.0055	zT_{xx} (0 T), 95.78 K	this work
NbP, Sample 1	Polycrystalline	0.0145	zT_{xxz} (9 T), 196.4 K	this work
NbP, Sample 1	Polycrystalline	0.0068	zT_{xyz} (9 T), 246.2 K	this work
NbP, Sample 1	**Polycrystalline**	**0.041**	**$zT_{\text{effective}}$ (9 T), 196.4 K**	**this work**
NbP, Sample 2	Polycrystalline	0.0027	zT_{xx} (0 T), 125.0 K	this work
NbP, Sample 2	Polycrystalline	0.0047	zT_{xxz} (9 T), 200.0 K	this work
NbP, Sample 2	Polycrystalline	0.023	zT_{xyz} (9 T), 250.0 K	this work
NbP, Sample 2	**Polycrystalline**	**0.039**	**$zT_{\text{effective}}$ (9 T), 250.0 K**	**this work**
NbP	Polycrystalline	0.0098	zT_{xyz} (9 T), 140 K	[2]
$Co_3Sn_2S_2$	Single crystal	0.0221	zT_{xx} (0 T), 180 K	[3]
TaAs	Single crystal	0.0135	zT_{xx} (0 T), 220 K	[28]
TaP	Single crystal	0.003252	zT_{xx} (0 T), 75 K	[29]
$MoTe_2$	Single crystal	0.00297	zT_{xx} (0 T), 20 K	[27]
$Mo_{0.92}Nb_{0.08}Te_2$	Single crystal	0.042	zT_{xx} (0 T), 80 K	[27]
$YbMnBi_2$	Single crystal	0.003252	zT_{xyz} (2 T), 180 K	[9]

applications in the other WSMs shown in Table II in their polycrystalline form.

Both the experimental and theoretical findings presented in the previous sections indicate that the TE properties of NbP are highly sensitive to changes in T_F and thus E_F, as TE transport is strongly dependent on the position of the chemical potential relative to the energy of the Weyl points. This sensitivity implies the possibility of tuning E_F of NbP and other type I WSMs to optimize TE properties at desirable operating conditions for devices. For the new proposed device of Fig. 9, maximizing the sum of $|S_{xxz}|$ and $|S_{xyz}|$ at the same temperature and magnetic field is desirable for ultimately maximizing $zT_{\text{effective}}$. This can be achieved by tuning T_F so that the maximum sum of $|S_{xxz}|$ and $|S_{xyz}|$ is observed based on desired device operating conditions of temperature and magnetic field. While the experimental data show only a comparison of two different Fermi temperatures, a theoretical model of the change in combined thermopower through deliberate tuning is shown in Fig. 11.

Figure 11 indicates that the sum $|S_{xxz}| + |S_{xyz}|$ depends significantly on T_F, the externally applied magnetic field, and the temperature. Again, we offer doping as a tuning mechanism to maximize the TE transport of a magnetic WSM TE device, where an appropriate value of T_F can be chosen to fit an application's operating magnetic field and temperature constraints.

VI. CONCLUSIONS

The TE properties of WSMs have been investigated recently as they offer insight into fundamental topological transport, but WSMs also innately demonstrate promise as TE materials themselves. Single crystals are typically considered to have the most impressive TE transport properties; however, single crystals are also costly, difficult to synthesize, and typically small and fragile. If WSMs are to be used in practical applications, polycrystalline samples are the cheaper and more durable option. Here, we find a simultaneously large

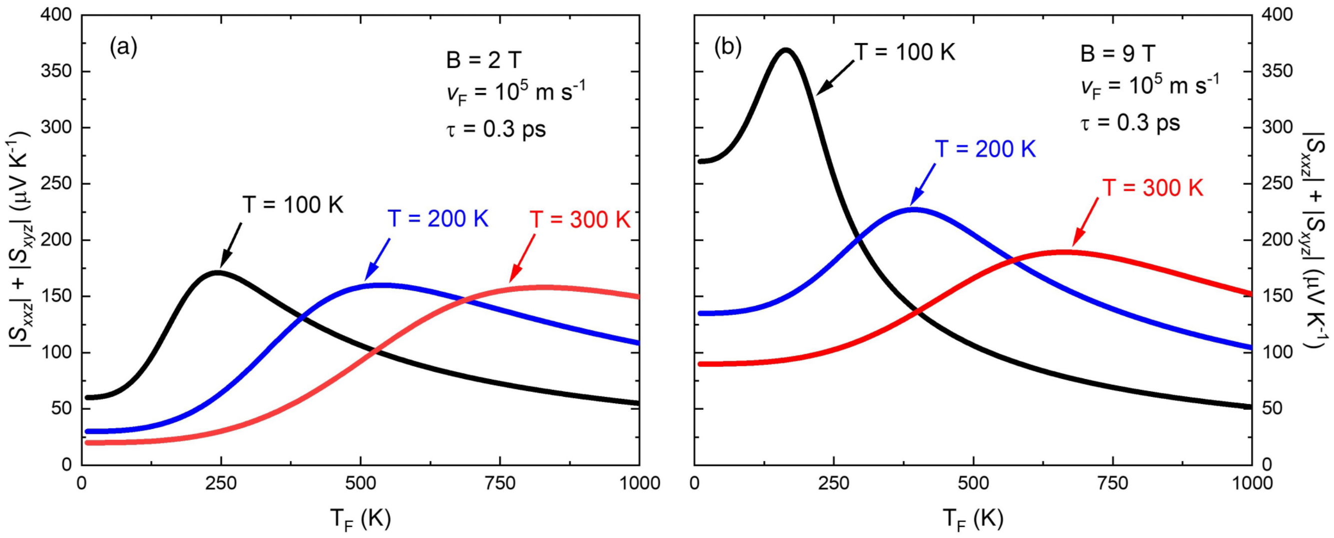

FIG. 11. Theoretical calculation of combined magnetic thermopowers ($|S_{xxz}| + |S_{xyz}|$) as a function of T_F at two externally applied discrete fields: (a) 2 T and (b) 9 T.

magneto-Seebeck and Nernst effect in two polycrystalline samples of NbP, with a significantly reduced thermal conductivity from that of single-crystalline values and reasonably low electrical resistivity, further indicating that magnetothermoelectric effects are an area of major interest in WSMs. When comparing experimental data to theoretical models, we have determined that TE effects in NbP are highly sensitive to doping, altering not only the maximum values of TE transport properties but the temperatures at which these maxima occur. We conclude that changes in the Fermi temperature through doping can be used as a sensitive tuning mechanism for TE properties and the temperatures at which they are maximized. Finally, because NbP possesses the unique simultaneous presence of both a large magneto-Seebeck and Nernst effect, we propose a device that utilizes both thermopowers produced in the presence of a magnetic field. The resulting zT of such a device was found to be significantly higher than the zT observed by the individual TE effects and is greater than zT found in other competitive WSMs. We offer all of this as evidence for the viability of polycrystalline WSMs in TE devices.

ACKNOWLEDGMENTS

E.F.S. and S.J.W. acknowledge support from the U.S. Department of Energy, Office of Science, Office of Basic Energy Sciences Early Career Research Program under Award No. DE-SC0020154. B.S. was supported in part by the NSF under Grant No. DMR-2045742. C.F. acknowledges support from the Fundamental Research Funds for the Central Universities.

[1] S. J. Watzman, T. M. McCormick, C. Shekhar, S. C. Wu, Y. Sun, A. Prakash, C. Felser, N. Trivedi, and J. P. Heremans, Dirac dispersion generates unusually large Nernst effect in Weyl semimetals, Phys. Rev. B **97**, 161404(R) (2018).

[2] C. Fu, S. N. Guin, S. J. Watzman, G. Li, E. Liu, N. Kumar, V. Su, W. Schnelle, G. Auffermann, C. Shekhar, Y. Sun, J. Gooth, and C. Felser, Large Nernst power factor over a broad temperature range in polycrystalline Weyl semimetal NbP, Energy Environ. Sci. **11**, 2813 (2018).

[3] S. N. Guin, V. P., Y. Zhang, N. Kumar, S. J. Watzman, C. Fu, E. Liu, K. Manna, W. Schnelle, J. Gooth, C. Shekhar, Y. Sun, and C. Felser, Zero-field nernst effect in a ferromagnetic Kagome-Lattice Weyl-semimetal $Co_3Sn_2S_2$, Adv. Mater. **31**, 1806622 (2019).

[4] R. Modak, K. Goto, S. Ueda, Y. Miura, K. Uchida, and Y. Sakuraba, Combinatorial tuning of electronic structure and thermoelectric properties in $Co_2MnAl_{1-x}Si_x$ Weyl semimetals, APL Mater. **9**, 031105 (2021).

[5] B. Peng, H. Zhang, H. Shao, H. Lu, D. W. Zhang, and H. Zhu, High thermoelectric performance of Weyl semimetal TaAs, Nano Energy **30**, 225 (2016).

[6] S. N. Guin, K. Manna, J. Noky, S. J. Watzman, C. Fu, N. Kumar, W. Schnelle, C. Shekhar, Y. Sun, J. Gooth, and C. Felser, Anomalous Nernst effect beyond the magnetization scaling relation in the ferromagnetic Heusler compound Co_2MnGa, NPG Asia Mater. **11**, 16 (2019).

[7] M. Ikhlas, T. Tomita, T. Koretsune, M. Suzuki, D. Nishio-Hamane, R. Arita, Y. Otani, and S. Nakatsuji, Large anomalous Nernst effect at room temperature in a chiral antiferromagnet, Nat. Phys. **13**, 1085 (2017).

[8] X. Li, L. Xu, L. Ding, J. Wang, M. Shen, X. Lu, Z. Zhu, and K. Behnia, Anomalous Nernst and Righi-Leduc Effects in Mn_3Sn: Berry Curvature and Entropy Flow, Phys. Rev. Lett. **119**, 056601 (2017).

[9] Y. Pan, C. Le, B. He, S. J. Watzman, M. Yao, J. Gooth, J. P. Heremans, Y. Sun, and C. Felser, Giant anomalous Nernst signal in the antiferromagnet $YbMnBi_2$, Nat. Mater. **21**, 203 (2022).

[10] H. Wang, X. Luo, W. Chen, N. Wang, B. Lei, F. Meng, C. Shang, L. Ma, T. Wu, X. Dai, Z. Wang, and X. Chen, Magnetic-field enhanced high-thermoelectric performance in topological Dirac semimetal Cd_3As_2 crystal, Sci. Bull. **63**, 411 (2018).

[11] J. Xiang, S. Hu, M. Lyu, W. Zhu, C. Ma, Z. Chen, F. Steglich, G. Chen, and P. Sun, Large transverse thermoelectric figure of merit in a topological Dirac semimetal, Sci. China-Phys. Mech. Astron. **63**, 237011 (2020).

[12] J. Hu, M. Caputo, E. Bonini Guedes, S. Tu, E. Martino, A. Magrez, H. Berger, J. H. Dil, H. Yu, and J. Anserme, Large magnetothermopower and anomalous Nernst effect in $HfTe_5$, Phys. Rev. B **100**, 115201 (2019).

[13] K. Tsuruda, K. Nakagawa, M. Ochi, K. Kuroki, M. Tokunaga, H. Murakawa, N. Hanasaki, and H. Sakai, Enhancing thermopower and nernst signal of high-mobility Dirac carriers by fermi level tuning in the layered magnet $EuMnBi_2$, Adv. Funct. Mater. **31**, 2102275 (2021).

[14] R. Lundgren, P. Laurell, and G. A. Fiete, Thermoelectric properties of Weyl and Dirac semimetals, Phys. Rev. B **90**, 165115 (2014).

[15] G. Sharma, P. Goswami, and S. Tewari, Nernst and magnetothermal conductivity in a lattice model of Weyl fermions, Phys. Rev. B **93**, 035116 (2016).

[16] E. H. Putley, *The Hall Effect and Related Phenomena* (Butterworths, London, 1960).

[17] S. Boona, H. Jin, and S. J. Watzman, Transverse thermal energy conversion using spin and topological structures, J. Appl. Phys. **130**, 171101 (2021).

[18] B. Skinner and L. Fu, Large, nonsaturating thermopower in a quantizing magnetic field, Sci. Adv. **4**, eaat2621 (2018).

[19] X. Feng and B. Skinner, Large enhancement of thermopower at low magnetic field in compensated semimetals, Phys. Rev. Mater. **5**, 024202 (2021).

[20] W. Liu, Z. Wang, J. Wang, H. Bai, Z. Li, J. Sun, X. Zhou, J. Luo, W. Wang, C. Zhang, J. Wu, Y. Sun, Z. Zhu, Q. Zhang, and X. Tang, Weyl semimetal states generated extraordinary quasi-linear magnetoresistance and nernst thermoelectric power factor in polycrystalline NbP, Adv. Funct. Mater. 2202143 (2022).

[21] C. Shekhar, A. K. Nayak, Y. Sun, M. Schmidt, M. Nicklas, I. Leermakers, U. Zeitler, Y. Skourski, J. Wosnitza, Z. Liu,

Y. Chen, W. Schnelle, H. Borrmann, Y. Grin, C. Felser, and B. Yan, Extremely large magnetoresistance and ultrahigh mobility in the topological Weyl semimetal candidate NbP, Nat. Phys. **11**, 645 (2015).

[22] See Supplemental Material at http://link.aps.org/supplemental/10.1103/PhysRevB.107.115108 for Hall effect measurements, calculation of the zero-Kelvin charge-carrier concentrations and mobilities, and further details on sample preparation and theoretical calculations.

[23] N. W. Ashcroft and N. D. Mermin, *Solid State Physics* (Holt, Rinehart, and Winston, New York, 1976).

[24] B. Skinner, Coulomb disorder in three-dimensional Dirac systems, Phys. Rev. B **90**, 060202(R) (2014).

[25] H. Weng, C. Fang, Z. Fang, B. A. Bernevig, and X. Dai, Weyl Semimetal Phase in Noncentrosymmetric Transition-Metal Monophosphides, Phys. Rev. X **5**, 011029 (2015).

[26] V. Kozii, B. Skinner, and L. Fu, Thermoelectric Hall conductivity and figure of merit in Dirac/Weyl materials, Phys. Rev. B **99**, 155123 (2019).

[27] H. Sakai, K. Ikeura, M. S. Bahramy, N. Ogawa, D. Hashizume, J. Fujioka, Y. Tokura, and S. Ishiwata, Critical enhancement of thermopower in a chemically tuned polar semimetal $MoTe_2$, Sci. Adv. **2**, e1601378 (2016).

[28] J. Xiang, S. Hu, M. Lv, J. Zhang, H. Zhao, G. Chen, W. Li, Z. Chen, and P. Sun, Anisotropic thermal and electrical transport of Weyl semimetal TaAs, J. Phys.: Condens. Matter **29**, 485501 (2017).

[29] F. Han, N. Andrejevic, T. Nguyen, V. Kozii, Q. T. Nguyen, T. Hogan, Z. Ding, R. Pablo-Pedro, S. Parjan, B. Skinner, A. Alatas, E. Alp, S. Chi, J. Fernandez-Baca, S. Huang, L. Fu, and M. Li, Quantized thermoelectric Hall effect induces giant power factor in a topological semimetal, Nat. Commun. **11**, 6167 (2020).